RESEARCH ARTICLE SUMMARY

CELL BIOLOGY

Reconstitution of autophagosome nucleation defines Atg9 vesicles as seeds for membrane formation

Justyna Sawa-Makarska*†, Verena Baumann*, Nicolas Coudevylle*, Sören von Bülow, Veronika Nogellova, Christine Abert, Martina Schuschnig, Martin Graef, Gerhard Hummer, Sascha Martens†

INTRODUCTION: Macroautophagy (hereafter autophagy) is an evolutionarily conserved lysosomal degradation pathway. It ensures cellular homeostasis and health by removing harmful material from the cytoplasm. Among the many substances that are degraded by autophagy are protein aggregates, damaged organelles, and pathogens. Defects in this pathway can result in diseases such as cancer and neurodegeneration. During autophagy, the harmful material, referred to as cargo, is sequestered by double-membrane vesicles called autophagosomes, which form de novo around the cargo. Autophagosome formation occurs at sites close to the endoplasmic reticulum (ER). The process is catalyzed by a complex machinery that includes protein and lipid kinases, membrane binding and transfer proteins, and ubiquitin-like conjugation systems. How these components and biochemical activities act in concert to mediate autophagosome formation is incompletely understood. Particularly enigmatic are autophagy related protein 9 (Atg9)–containing vesicles that are required for the assembly of the autophagy machinery but do not supply the bulk of the autophagosomal membrane.

RATIONALE: To understand the mechanism of how the various biochemical activities of the autophagy machinery are orchestrated during the nucleation and expansion of the precursors to autophagosomes at the cargo, we fully reconstituted these events using the yeast machinery. Specifically, we used recombinantly expressed and purified proteins in combination with reconstituted Atg9 proteoliposomes and endogenous Atg9 vesicles isolated from cells. Our reconstituted system included 21 polypeptides, as well as membrane platforms, making up almost the entire yeast core machinery required for selective autophagy. This approach allowed us to exert full control over the biochemical reactions and to define the organization principles of the early autophagy machinery.

RESULTS: We found that Atg9 vesicles and proteoliposomes were recruited to the autophagy cargo via the Atg19 receptor and Atg11 scaffold axis. The vesicles in turn recruited the Atg2-Atg18 lipid transfer complex and the class III phosphatidylinositol 3-phosphate kinase complex 1(PI3KC3-C1), which produced the signaling lipid phosphatidylinositol 3-phosphate (PI3P). PI3P production triggered the subsequent recruitment of the PI3P-binding protein Atg21, which together with the Atg2-Atg18 complex efficiently attracted the E3-like Atg12–Atg5-Atg16 complex. Together with the E1-like Atg7 and the E2-like Atg3 proteins, the recruitment of the E3-like complex ultimately resulted in the conjugation of the ubiquitin-like Atg8 protein to the headgroup of phosphatidylethanolamine (PE) on the Atg9 vesicles and proteoliposomes. Atg8 conjugation is a hallmark of autophagy and necessary for membrane expansion. Furthermore, we discovered that sustained Atg8 conjugation required the Atg2-mediated transfer of PE from a donor membrane into Atg9 proteoliposomes.

CONCLUSION: We conclude that Atg9 vesicles form seeds that establish membrane contact sites to initiate the transfer of lipids from donor compartments such as the ER. It has become increasingly clear that lipid transport between different compartments occurs at membrane contact sites and that it is mediated by lipid transfer proteins. Notably, lipid transfer at membrane contact sites requires two preexisting compartments. We propose that during the de novo formation of autophagosomes, the Atg9 vesicles recruit the autophagy machinery and serve as nucleators to establish membrane contact sites with a donor compartment such as the ER. Atg2-mediated lipid transfer in conjunction with energy-consuming reactions such as PI3K-dependent PI3P production and Atg8 lipidation on the Atg9 vesicles drive net flow of lipids into the vesicles, resulting in their expansion for autophagosome formation. ■

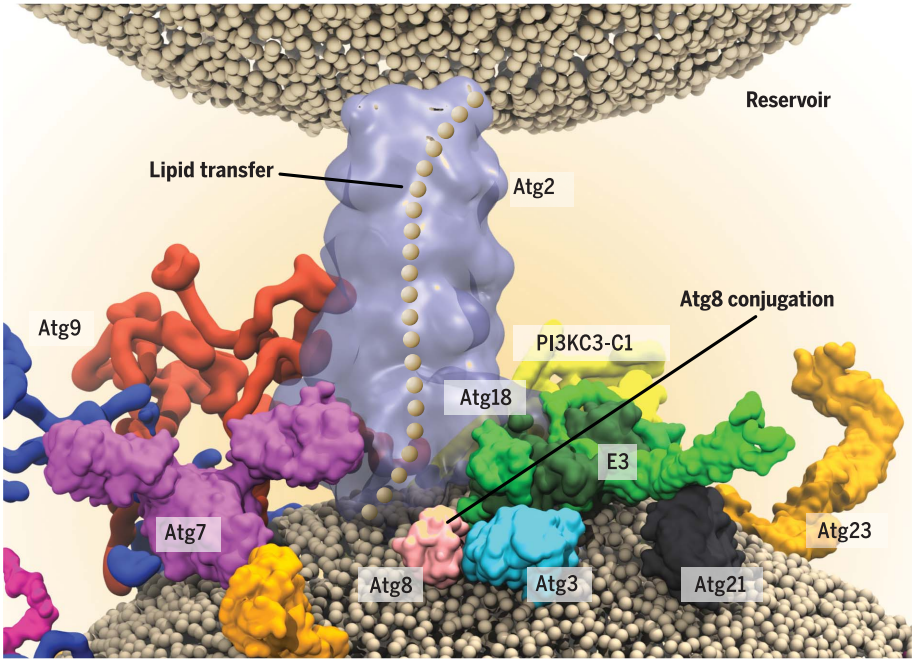

Assembly of the yeast autophagy machinery. Model for the assembly of the yeast autophagy machinery and Atg2-mediated lipid transfer into Atg9 vesicles from a donor compartment, such as the endoplasmic reticulum, during the nucleation of autophagosomes.

The list of author affiliations is available in the full article online.
*These authors contributed equally to this work.
†Corresponding author. Email: justyna.sawa-makarska@univie.ac.at (J.S.-M.); sascha.martens@univie.ac.at (S.M.)
Cite this article as J. Sawa-Makarska *et al.*, *Science* **369**, eaaz7714 (2020). DOI: 10.1126/science.aaz7714

READ THE FULL ARTICLE AT
https://doi.org/10.1126/science.aaz7714

RESEARCH ARTICLE

CELL BIOLOGY

Reconstitution of autophagosome nucleation defines Atg9 vesicles as seeds for membrane formation

Justyna Sawa-Makarska[1]*†, Verena Baumann[1]*, Nicolas Coudevylle[1]*, Sören von Bülow[2], Veronika Nogellova[1], Christine Abert[1], Martina Schuschnig[1], Martin Graef[3,4], Gerhard Hummer[2,5], Sascha Martens[1]†

Autophagosomes form de novo in a manner that is incompletely understood. Particularly enigmatic are autophagy-related protein 9 (Atg9)–containing vesicles that are required for autophagy machinery assembly but do not supply the bulk of the autophagosomal membrane. In this study, we reconstituted autophagosome nucleation using recombinant components from yeast. We found that Atg9 proteoliposomes first recruited the phosphatidylinositol 3-phosphate kinase complex, followed by Atg21, the Atg2-Atg18 lipid transfer complex, and the E3-like Atg12–Atg5-Atg16 complex, which promoted Atg8 lipidation. Furthermore, we found that Atg2 could transfer lipids for Atg8 lipidation. In selective autophagy, these reactions could potentially be coupled to the cargo via the Atg19-Atg11-Atg9 interactions. We thus propose that Atg9 vesicles form seeds that establish membrane contact sites to initiate lipid transfer from compartments such as the endoplasmic reticulum.

Autophagy mediates the degradation of cytoplasmic material (the cargo) within lysosomes and ensures cellular homeostasis (*1*). Defects in autophagy have been associated with severe pathologies such as neurodegeneration, cancer, and infections (*2*). Cargo degradation is achieved by its sequestration within double-membrane vesicles called autophagosomes. These form de novo in an inducible manner and first appear as small membrane structures called isolation membranes (or phagophores), which gradually enclose the cargo as they grow. The assembly and growth of the isolation membranes is dependent on a number of conserved autophagy-related (Atg) proteins that act together in a hierarchical manner to nucleate and expand the isolation membranes (*3*–*5*). In yeast, these include the Atg1 protein kinase complex, vesicles containing the Atg9 protein, the class III phosphatidylinositol 3-phosphate kinase complex 1 (PI3KC3-C1) producing the signaling lipid phosphatidylinositol 3-phosphate (PI3P), the PI3P-binding PROPPIN proteins, the lipid transfer protein Atg2, and the ubiquitin-like Atg12 and Atg8 conjugation systems (Fig. 1A). During selective autophagy, the interaction of cargo receptors with scaffold proteins directs this machinery toward specific cargos (*6*, *7*). The attachment of Atg8 to the membrane lipid phosphatidylethanolamine (PE), referred to as lipidation, is the most downstream event of this cascade. How the biochemical activities of the autophagy machinery are orchestrated to mediate the formation of autophagosomes is not well understood. Especially enigmatic is the role of Golgi-derived Atg9 vesicles that are required for nucleation of the isolation membrane but that do not provide the bulk of the autophagosomal membrane (*8*–*11*). The bulk of the lipids appears to be derived from other donor compartments, in particular the endoplasmic reticulum (ER) (*12*–*19*).

Previous work has demonstrated that membrane contact sites are major mediators of nonvesicular lipid flow between compartments within the cell (*20*, *21*). The flow of lipids is mediated by lipid transfer proteins that extract lipids from a donor membrane and transport them to an acceptor membrane. To elucidate how the various activities of the autophagy machinery act together during the nucleation of isolation membranes, we reconstituted a large part of the yeast autophagy machinery in vitro.

Membrane recruitment of Atg12–Atg5-Atg16 by Atg21 and Atg2-Atg18

A hallmark of isolation membranes and completed autophagosomes is the conjugation of the ubiquitin-like Atg8 proteins to the headgroup of the lipid PE (*22*, *23*). The Atg8 proteins are required for isolation membrane expansion, closure, and cargo selectivity (*24*). The conjugation of Atg8 to PE is mediated by the E1-like Atg7 and the E2-like Atg3 proteins (*22*) as well as the Atg12–Atg5-Atg16 complex that acts in an E3-like manner (*25*) by activating and localizing Atg8-loaded Atg3 to the membrane (*26*, *27*). Thus, the localization of the Atg12–Atg5-Atg16 complex is a crucial determinant of the site of Atg8 lipidation (*28*). Atg16 binds to the PI3P-binding PROPPIN protein Atg21 (*29*). We sought to determine whether this interaction could mediate the recruitment of the Atg12–Atg5-Atg16 complex to PI3P-containing membranes, such as the isolation membrane, and found that Atg21 bound to PI3P-containing giant unilamellar vesicles (GUVs) (Fig. 1B). As expected (*27*), the Atg12–Atg5-Atg16 complex did not directly bind to this lipid composition and was recruited only in the presence of Atg21 (Fig. 1B). In cells, the PI3P at the pre-autophagosomal structure (PAS) recruits another PROPPIN, the Atg18 protein in complex with the membrane tethering and lipid transfer protein Atg2 (*16*, *30*–*33*). We examined whether the Atg2-Atg18 complex could also interact with Atg12–Atg5-Atg16 and thereby contribute to its recruitment to PI3P-positive membranes. Indeed, we detected a direct interaction between the two protein complexes in a pull-down assay (Fig. 1C). We also observed that the presence of Atg2-Atg18 tended to accelerate the recruitment of the Atg12–Atg5-Atg16 complex to PI3P-containing GUVs (fig. S1A). Microscopy-based pull-down and membrane recruitment experiments indicated that, as expected, Atg21 bound to the Atg12–Atg5-Atg16 complex via Atg16 (fig. S1, B and C) (*29*), while the interaction of Atg2 was mediated by Atg5 and the interaction of Atg18 required the presence of Atg12 (Fig. 1, D to F, and fig. S1D).

These results suggested the formation of a holocomplex on the membrane, containing Atg21, Atg12–Atg5-Atg16, and Atg2-Atg18, and so we dissected the recruitment of the individual components in more detail. Atg21 was the main driving force for the recruitment of Atg12–Atg5-Atg16 under the conditions tested (Fig. 1G). In cells, both PROPPINS (Atg18 and Atg21) and Atg2 contributed to the localization of Atg12–Atg5-Atg16 to the PAS (fig. S2) (*29*). The residual recruitment of Atg12–Atg5-Atg16 in the triple-deficient cells could be mediated by the Atg1 complex (*34*). In addition, deletion of Atg2, Atg18, and Atg21 strongly reduced Atg8 lipidation (fig. S3A), and deletion of any of the three proteins stalled the progression of the autophagic pathway (fig. S3, B and C) (*29*, *30*).

At the PAS, the PI3KC3-C1 [consisting of the vacuolar protein sorting 34 (Vps34), Vps15, Atg6, and Atg14 subunits] phosphorylates phosphatidylinositol (PI) to PI3P (*35*). To address whether the recruitment of the Atg12–Atg5-Atg16 complex and Atg8 lipidation could be driven by the activity of the PI3KC3-C1 through the PI3P-dependent recruitment of Atg2-Atg18 and Atg21, we added the purified PI3KC3-C1 to PI-containing GUVs in the presence of Atg21 and Atg2-Atg18 (Fig. 2A). The Atg12–Atg5-Atg16

[1]Department of Biochemistry and Cell Biology, Max Perutz Labs, University of Vienna, 1030 Vienna, Austria. [2]Department of Theoretical Biophysics, Max Planck Institute of Biophysics, 60438 Frankfurt am Main, Germany. [3]Max Planck Institute for Biology of Ageing, 50931 Cologne, Germany. [4]Cologne Excellence Cluster on Cellular Stress Responses in Aging-Associated Diseases (CECAD), University of Cologne, 50931 Cologne, Germany. [5]Institute for Biophysics, Goethe University Frankfurt, 60438 Frankfurt am Main, Germany.
*These authors contributed equally to this work.
†Corresponding author. Email: justyna.sawa-makarska@univie.ac.at (J.S.-M.); sascha.martens@univie.ac.at (S.M.)

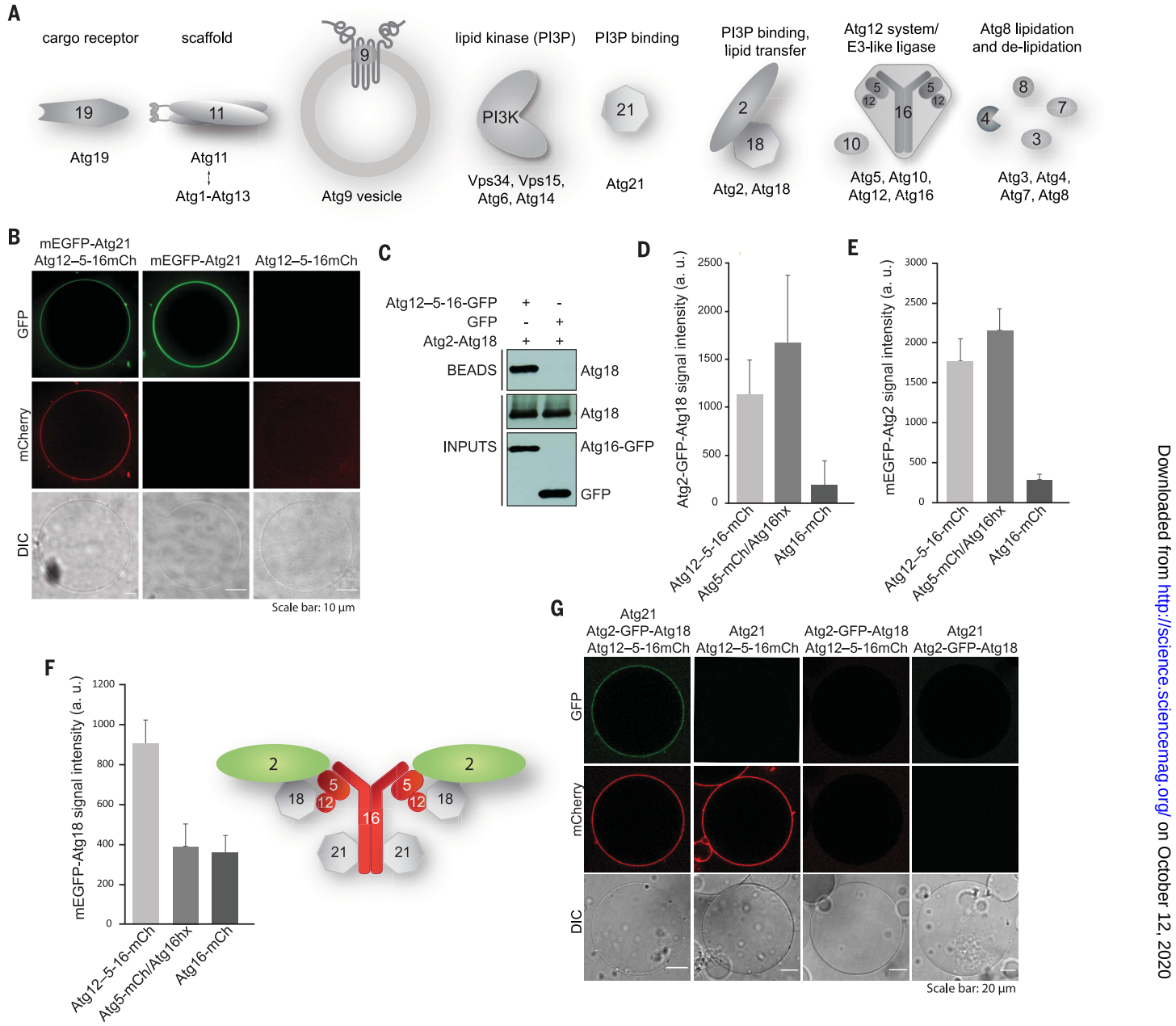

Fig. 1. Membrane recruitment of the Atg12–Atg5-Atg16 complex by PROPPINs. (**A**) Cartoon showing proteins used in this study. PI3KC3-C1 is labeled as PI3K in all figures. (**B**) GUVs containing PI3P (57% POPC, 25.5% POPS, 15% POPE, 2.5% PI3P; see table S2 for lipid definitions) were incubated with either 1 μM Atg12–Atg5-Atg16-mCherry supplemented with 1 μM eGFP-Atg21, 1 μM eGFP-Atg21, or 1 μM Atg12–Atg5-Atg16-mCherry and imaged by microscopy. DIC, differential interference contrast microscopy. (**C**) GFP-Trap pulldown using Atg12–Atg5-Atg16-GFP or GFP as bait and Atg2-Atg18 as prey. The bait and the prey proteins were detected by immunoblotting with anti-GFP and anti-CBP antibodies, respectively. (**D** to **F**) Quantification of the pull-down experiment mapping the interaction between Atg12–Atg5-Atg16 and Atg2-Atg18 shown in fig. S1D. The quantification is based on three independent experiments. Standard deviations are shown. A schematic representation of the putative holocomplex composed of Atg12–Atg5-Atg16, Atg2-Atg18, and Atg21 is shown as a cartoon insert in (F). a.u., arbitrary units. (**G**) GUVs of the same lipid composition as in (B) were incubated with Atg12–Atg5-Atg16-mCherry, Atg21, or Atg2-GFP-Atg18 at 1 μM final concentration each, and the recruitment of the proteins to the membrane was imaged by microscopy.

complex was recruited to the GUV membrane, and this recruitment was dependent on the activity of the PI3KC3-C1 (Fig. 2A and fig. S4A). Atg21 alone was sufficient to recruit the Atg12–Atg5-Atg16 complex and to induce Atg8 lipidation on the GUVs (Fig. 2B). These effects were enhanced when Atg2-Atg18 was also present (Fig. 2B). We interpreted the localization of green fluorescent protein (GFP)–Atg8 on the membrane as lipidation because it was abolished when using a nonconjugatable form of Atg8 (GFP-Atg8-6xHis) and it strictly depended on the presence of the conjugation machinery Atg7 and Atg3 (fig. S4B).

Reconstitution of Atg8 lipidation on Atg9 proteoliposomes

Autophagosome nucleation depends on the presence of Atg9 vesicles (*8*–*11*). In *Saccharomyces cerevisiae*, a few of these vesicles translocate to the autophagosome formation site (*8*). Because Atg9 is required for the recruitment of

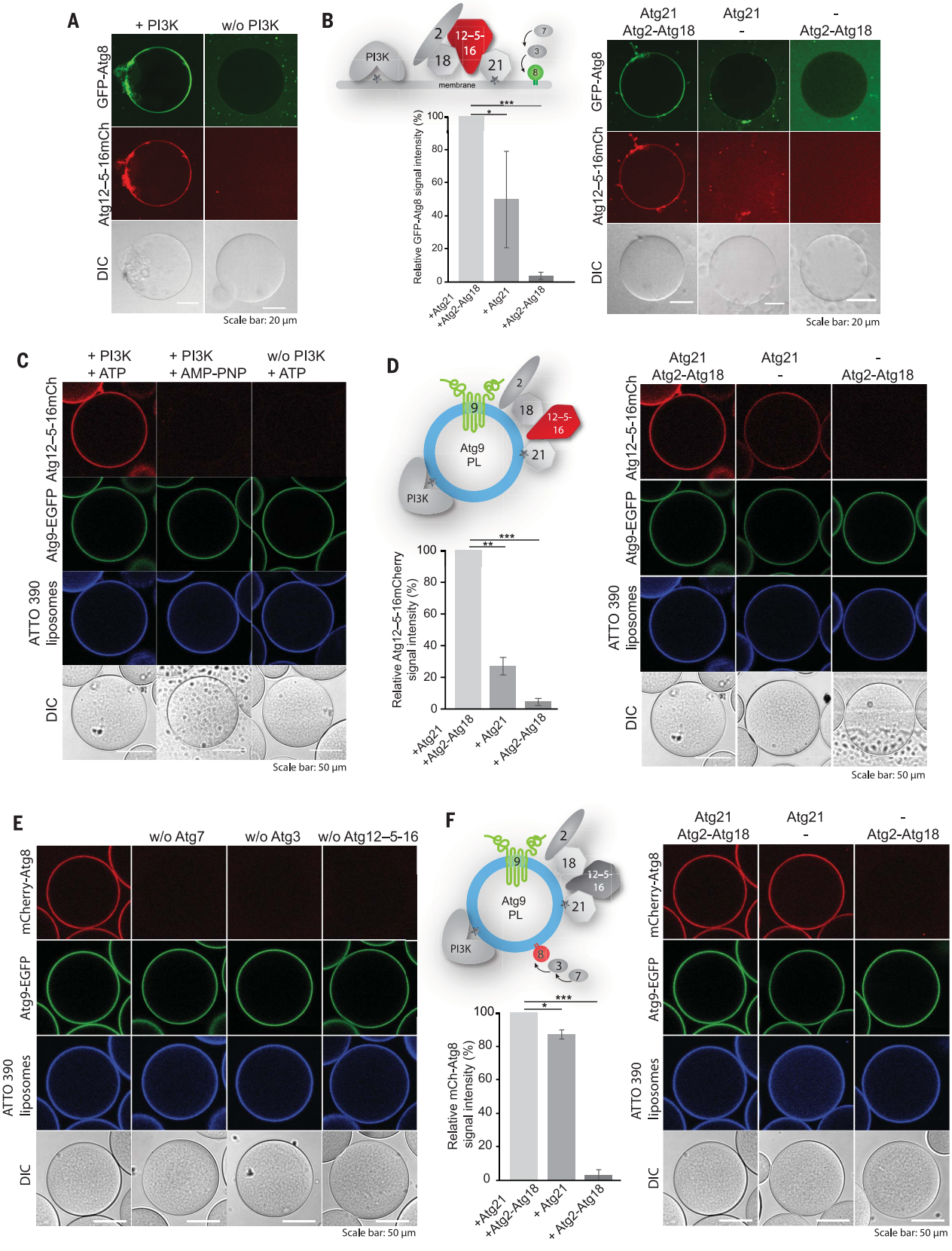

Fig. 2. In vitro reconstitution of PI3KC3-C1–dependent Atg8 lipidation. (**A**) The Atg8–PE conjugation machinery (Atg7, Atg3, Atg12–Atg5-Atg16-mCherry, and GFP-Atg8ΔR117) and PROPPINs (Atg21 and Atg2-Atg18) were added to GUVs (55% DOPC, 10% DOPS, 17% DOPE, 18% liver PI) and incubated in the presence or absence of PI3KC3-C1 and cofactors (ATP, $MnCl_2$, $MgCl_2$, and EGTA). Microscopy images of representative GUVs are shown. The proteins included in the experiment are depicted in the cartoon inserts. (**B**) Atg8 lipidation to GUVs depends on the presence of Atg21. GUVs were incubated with Atg8–PE conjugation machinery proteins as in (A) and PI3KC3-C1 in the presence of either one or both PROPPINs. The quantification of the GFP signal on GUVs from three independent experiments is shown to the left. (**C**) Atg12–Atg5-Atg16 recruitment to Atg9 PLs depends on the activity of PI3KC3-C1. GFP-Trap beads were coated with Atg9-EGFP PLs and incubated with Atg21, Atg2-Atg18, and Atg12–Atg5-Atg16-mCherry in the presence or absence of PI3KC3-C1 and ATP or in the presence of PI3KC3-C1 and AMP-PNP. Microscopy images of representative beads are shown. (**D**) Beads as in (C) were incubated with Atg12–Atg5-Atg16-mCherry and PI3KC3-C1 in the presence of either one or both PROPPINs. The quantification of mCherry signal on beads from three independent experiments is shown to the left. (**E**) Reconstitution of Atg8 lipidation to Atg9 PLs. Beads as in (C) were incubated with PI3KC3-C1, ATP, Atg21, Atg2-Atg18, mCherry-Atg8ΔR117, Atg7, Atg3, and Atg12–Atg5-Atg16, each time omitting one of the Atg8–PE conjugation machinery proteins, as indicated above the microscopy images of representative beads. (**F**) Atg8 lipidation to Atg9 PLs depends on the presence of Atg21. Beads as in (C) were incubated with PI3KC3-C1, ATP, mCherry-Atg8ΔR117, Atg7, Atg3, and Atg12–Atg5-Atg16 in the presence of either one or both PROPPINs. The quantification of mCherry signal on the beads from three independent experiments is shown to the left. Significance is indicated using *P* values from Student's *t* test: $*P \le 0.05$, $**P \le 0.01$, $***P \le 0.001$.

the PI3KC3-C1 to the site of autophagosome formation (*36*), we wondered whether the Atg9 vesicles could serve as platforms for the assembly of the autophagy machinery and thereby nucleate autophagosome formation. To this end, we reconstituted the purified Atg9 protein into small unilamellar vesicles (SUVs) to form proteoliposomes (PLs) (fig. S5, A to D). To mimic the natural lipid composition of these vesicles, we isolated Atg9 vesicles from *S. cerevisiae* and determined their lipid composition by lipidomics (fig. S6A). The vesicles had a high PI content (44%) (fig. S6B) (*37*), suggesting that they should be particularly good substrates for the PI3KC3-C1. To test this, we tethered PLs containing Atg9–enhanced green fluorescent protein (EGFP) to GFP-Trap beads to image the recruitment of other factors by microscopy. The membrane of the PLs was labeled by incorporation of a blue membrane dye (ATTO390-DOPE). Upon incubation of the vesicles with the PI3KC3-C1, Atg21, Atg2-Atg18, and the Atg12–Atg5-Atg16 complex, we observed recruitment of Atg12–Atg5-Atg16 to the Atg9 PLs (Fig. 2C). Consistent with the results above (Figs. 1G and 2B), recruitment was strongest in the presence of both Atg2-Atg18 and Atg21 (Fig. 2D). We then added Atg7 and Atg3 to the reaction (now containing 14 polypeptides) to test whether Atg8 could be conjugated to the Atg9 PLs in a manner that depends on PI3KC3-C1, Atg21, Atg2-Atg18, and Atg12–Atg5-Atg16. We observed efficient Atg8 lipidation to the Atg9 PLs (Fig. 2E). Reduction of the Atg8 signal upon addition of the wild-type delipidating enzyme Atg4 but not its catalytic mutant (fig. S7A) showed that the detected mCherry-Atg8 signal at the beads was indeed attributable to lipidation.

Analogous to the results we observed for Atg12–Atg5-Atg16 recruitment, Atg8 conjugation was relatively independent of the Atg2-Atg18 complex and was also weakly detectable in the absence of the PI3KC3-C1 (Fig. 2F and fig. S7, B and C), likely because Atg21 shows residual binding to PI-containing membranes. These results suggested a division of labor between Atg21 and Atg2-Atg18, where Atg21 plays a major role in the initial recruitment of Atg12–Atg5-Atg16, and the main function of Atg2-Atg18 could be membrane tethering and lipid transfer (*16*, *30*–*33*).

Reconstitution of autophagosome nucleation in selective autophagy

In selective autophagy, autophagosome nucleation must be coupled to the presence of cargo material (*7*). The cargo is recognized by cargo receptors such as p62 in human cells and Atg19 in *S. cerevisiae*. These cargo receptors link the autophagy machinery to the cargo via the FIP200/Atg11 proteins (*6*). Atg11 was shown to interact with Atg9 (*38*, *39*). We purified full-length Atg11 and, in agreement with (*40*) but in contrast to (*39*), found Atg11 to be a constitutive dimer (fig. S8B). Atg11 bound directly to the N terminus of Atg9 (fig. S8C). Next, we examined whether the Atg19 cargo receptor could recruit the autophagy machinery, including Atg9 vesicles, to the cargo and subsequently initiate Atg8 conjugation. The cargo was mimicked by attachment of the GST-prApe1 propeptide (residues 1 to 41) to glutathione beads. These were incubated with the Atg19 cargo receptor and subsequently with Atg11. Atg11 was recruited to the beads in an Atg19-dependent manner. The recruitment was enhanced when a phospho-mimicking mutant of Atg19 [$Ser^{390,391,396}$→Asp (S390D, S391D, and S396D)] (*41*) was used (fig. S8A). Atg9 PLs and Atg9 vesicles isolated from cells (fig. S9) bound to the cargo beads in an Atg11-dependent manner (Fig. 3, A and B, and fig. S8D). When we added the PI3KC3-C1, Atg2-Atg18, Atg21, Atg12–Atg5-Atg16, Atg3, Atg7, and Atg8 to the Atg9 PLs bound to the cargo beads—a reaction now containing almost the entire autophagy machinery—Atg8 was efficiently lipidated and anchored to the Atg9 PLs (Fig. 3C). Isolated Atg9 vesicles could also serve as substrates for the lipidation reaction (Fig. 3D), although the lipidation was markedly less prominent on the vesicles than on the reconstituted PLs (fig. S10A). The Atg8 signal on the Atg9 vesicles was attributable to lipidation because it depended on the Atg12–Atg5-Atg16 complex (Fig. 3D) and decreased upon addition of Atg4 (Fig. 3E). Thus, the autophagy machinery can be redirected toward the cargo via the cargo receptor (Atg19)–scaffold (Atg11)–Atg9 axis (Fig. 3 and fig. S10B). The Atg1-Atg13 complex was also recruited to these beads (fig. S10C). Thus, Atg11 and Atg9 vesicles are sufficient to recruit (almost) the entire autophagy machinery to the cargo.

Atg9 vesicles as acceptors for lipid transfer by Atg2

Owing to their small size, Atg9 vesicles provide only limited surface for Atg8 lipidation and isolation membrane expansion. Furthermore, in addition to Atg9, these vesicles contain other proteins, which further reduce the effective surface for lipidation. This is consistent with our finding that Atg9 vesicles were less efficient substrates for Atg8 lipidation than Atg9 PLs (Fig. 3 and fig. S10A). To estimate the available membrane surface of these vesicles, we built a three-dimensional model of an Atg9 vesicle (Fig. 4A and movie S1). We based this model on an average diameter of 60 nm (fig. S9) (*8*), our proteomics data (fig. S6C and data S1), and an average of 28 Atg9 molecules per vesicle (*8*). In addition, we placed one molecule each of PI3KC3-C1, Atg2-Atg18, Atg21, Atg12–Atg5-Atg16, and Atg3 loaded with Atg8 on the vesicular membrane (see Materials and methods section for details). With 70 proteins present in the modeled Atg9 vesicle, the accessibility of the membrane would be very limited. We calculated an effective dynamic surface coverage of 82% of the membrane area. Given that peripheral membrane proteins may have been lost during the isolation, the very stringent selection of proteins from mass spectrometric data used for modeling, and the fact that we assumed the Atg9 N and C termini not to interact with the vesicular membrane, the actual free surface may be even lower and more difficult to reach for incoming proteins. Thus, Atg9 vesicles may require lipid influx to transform into an efficient substrate for Atg8 lipidation.

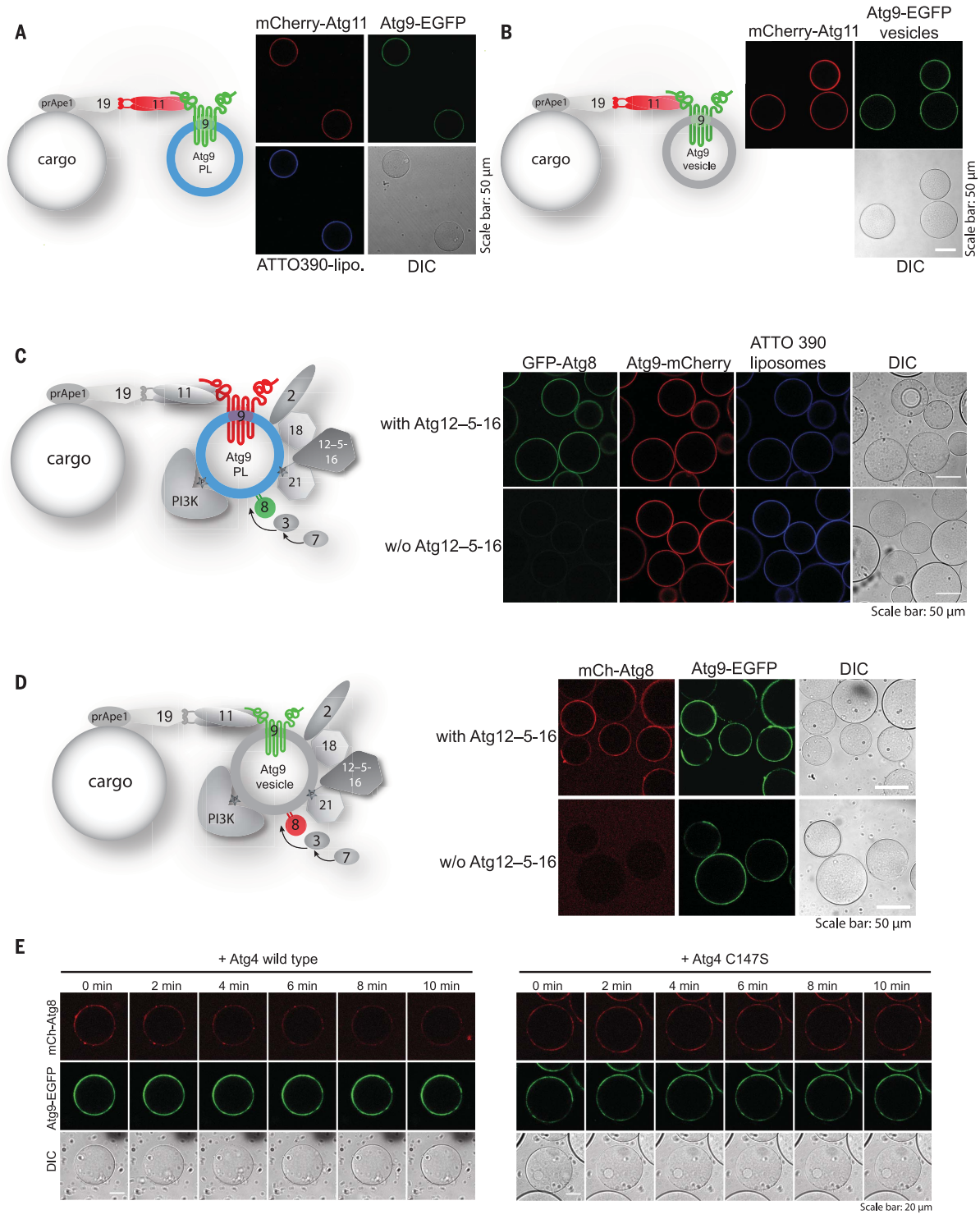

Fig. 3. Reconstitution of cargo-directed Atg8 lipidation to Atg9 PLs and Atg9 endogenous vesicles. (**A** and **B**) Recruitment of Atg PLs and endogenous Atg9 vesicles to the cargo. Cargo-mimetic beads (glutathione sepharose) were prepared by coating with GST-prApe1 (1-41), Atg19-3D, and mCherry-Atg11. For details of the pull-down, see fig. S8A. The preassembled cargo-mimetic beads were subsequently incubated with either Atg9-EGFP PLs (A) or endogenous Atg9-EGFP vesicles (B), washed, and imaged. Microscopy images of representative beads are shown. The Atg9-eGFP PLs were additionally labeled with ATTO390-PE. The experimental setup is shown by the accompanying cartoons. (**C** and **D**) Atg8-lipidation on the Atg9 PLs (C) and endogenous Atg9 vesicles (D) bound to the cargo-mimetic beads. Glutathione sepharose beads were coated with GST-prApe1 (1-41), Atg19-3D, and Atg11, incubated with Atg9-mCherry PLs (C) or Atg9-EGFP vesicles (D), washed with buffer, and incubated with PI3KC3-C1, ATP, Atg21, Atg2-Atg18, Atg3, Atg12–Atg5-Atg16, eGFP-Atg8ΔR117 (C) or mCherry-Atg8ΔR117 (D) and with or without Atg12–Atg5-Atg16 (see cartoons for the experimental setup). Microscopy images of representative beads are shown. (**E**) Time course experiment of the Atg8-deconjugation reaction on Atg9 vesicles. Atg4 wild type or the Atg4 C147S inactive mutant were added to the beads, as in (D). Microscopy images were taken at the indicated time points after the addition of Atg4.

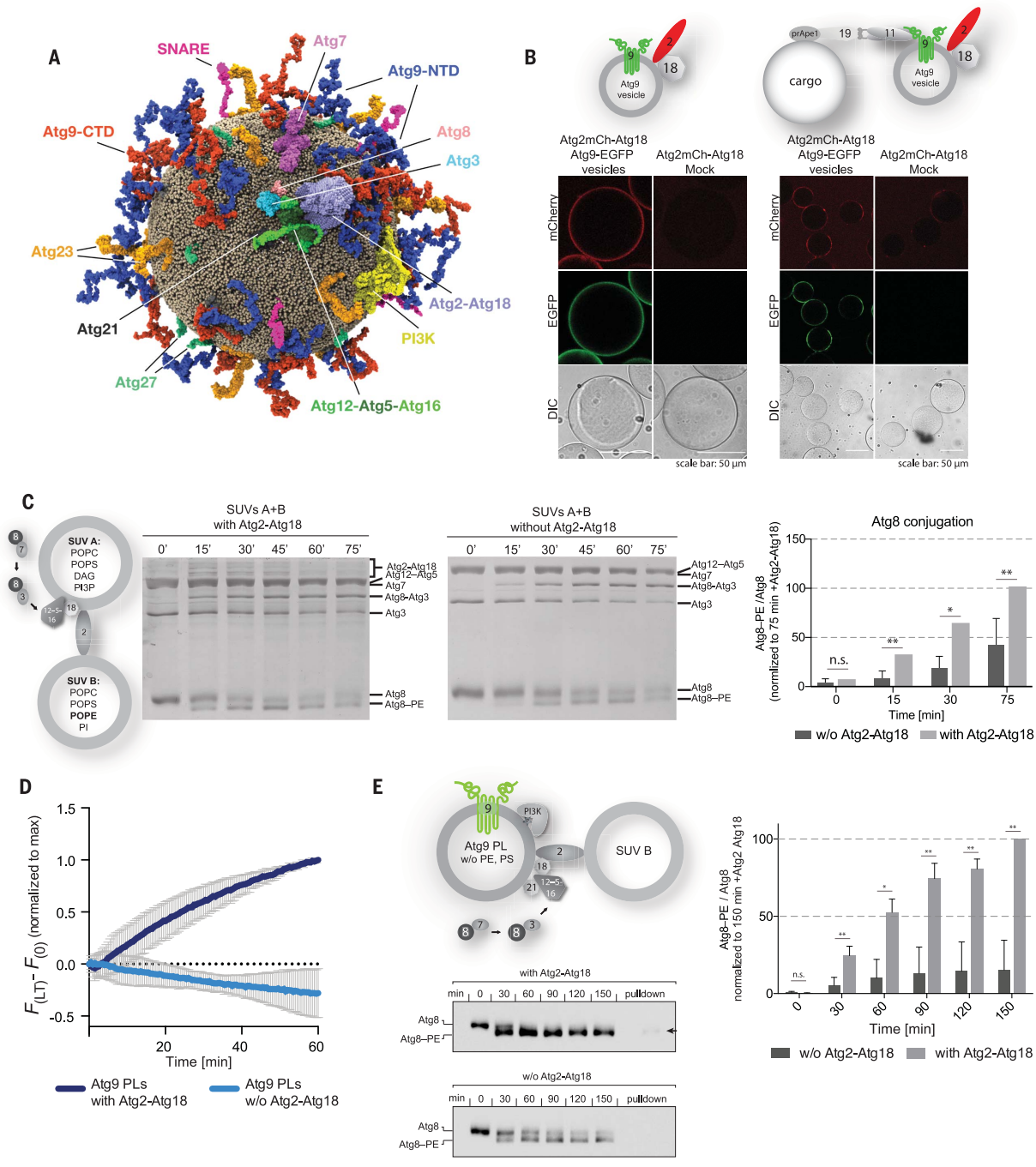

Fig. 4. Atg2-mediated lipid transfer into Atg9 PLs. (**A**) Molecular model of an endogenous Atg9 vesicle. The model contains the following proteins (copy numbers in parentheses): Atg9 (28), Atg27 (10), Atg23 (10), and the SNAP receptors (SNAREs) SFT1 (1), TLG1 (1), VTI1 (1), SSO1 (1), and GOS1 (1). Copy numbers are based on literature and mass spectrometry analysis of isolated Atg9 vesicles (see main text, fig. S6C, and methods section). Single copies of membrane-interacting autophagy proteins (PI3KC3-C1, Atg21, Atg2-Atg18, Atg3, Atg12–Atg5-Atg16, and Atg8) were additionally positioned on the surface of the Atg9 vesicle. Atg9-NTD and Atg9-CTD indicate N-terminal and C-terminal domains, respectively. Lipid headgroups are shown as small tan spheres. (**B**) Atg2-Atg18 is recruited to Atg9 vesicles and cargo-mimetic beads. GFP-Trap beads were coated with endogenous Atg9-EGFP vesicles. Glutathione sepharose beads were coated with GST-prApe1 (1-41), Atg19-3D, Atg11, and Atg9-EGFP vesicles and incubated with Atg2-mCherry-Atg18. Mock membranes were derived from a wild-type yeast strain. (**C**) Coomassie-stained gels showing Atg8–PE conjugation assays using the depicted experimental setup. Atg8–PE conjugation was detected as a band shift. Numbers above the gels indicate the time in minutes. (**D**) Phospholipid transfer assay based on the dequenching of NBD fluorescence. $F_{(LT)}$ and $F_{(0)}$ represent the nitrobenzoxadiazole (NBD) fluorescence intensity at each time point after and before addition of Atg2-Atg18, respectively, measured at 535 nm. Atg9 PLs were used as acceptor liposomes. Data are the mean values from five independent experiments. SD is shown. (**E**) Anti-Atg8 immunoblots showing Atg8–PE conjugation assays mediated by lipid transfer of Atg2-Atg18. The arrow indicates the Atg8 signal after pulling down Atg9-EGFP with GFP-Trap beads. [(C) and (E)] Quantification shows the averaged Atg8-PE/Atg8 ratio for each time point. Error bars represent SD. The quantification is based on four independent experiments. *P* values were calculated using Student's *t* test. Significance is indicated with $*P \leq 0.05$ and $**P \leq 0.01$ n.s., not significant.

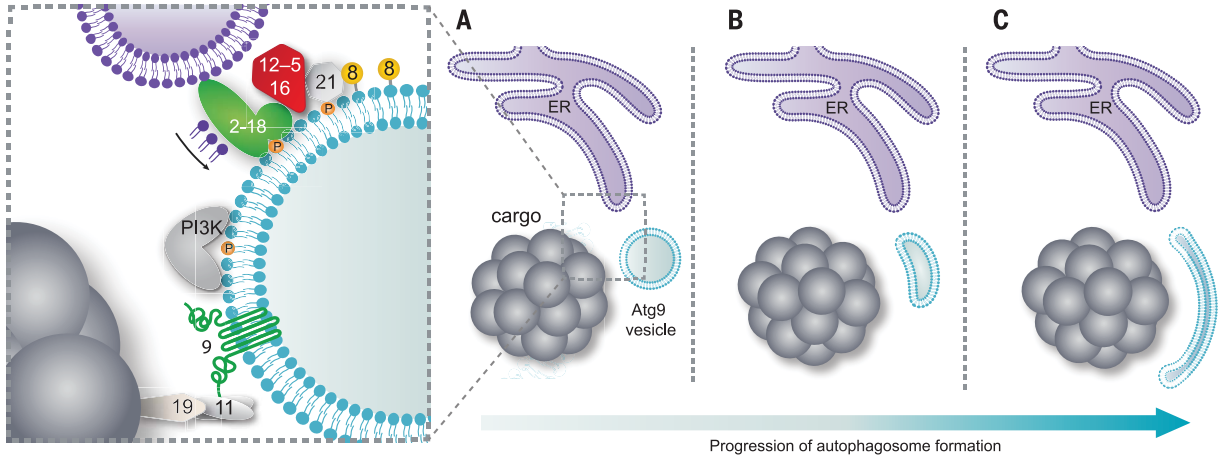

Fig. 5. Model for the initial steps of the isolation membrane generation. (**A**) Recruitment of Atg9 vesicles to the prApe1 cargo via the Atg19 receptor and Atg11 scaffold axis. The Atg9 vesicles recruit Atg2-Atg18 and PI3KC3-C1 (labeled PI3K). Production of PI3P by PI3KC3-C1 recruits Atg21 and the E3-like Atg12–Atg5-Atg16 complex. The membrane-positioned E3-like complex directs Atg8–PE conjugation to the vesicle. Atg8 lipidation is sustained by Atg2-mediated lipid transfer from a donor compartment such as the ER. (**B** and **C**) Lipid influx expands the vesicle surface resulting in isolation membrane expansion.

The lipid transfer protein Atg2 is recruited to the Atg9 vesicles (Fig. 4B) and tethers Atg9 to the ER in cells (*16*). The interaction between ATG2A and ATG9A is important for isolation membrane expansion in mammalian cells (*42*). Atg2-mediated lipid transfer from the ER into the membrane of the Atg9 vesicle may therefore enable Atg8 lipidation and subsequent expansion of the spherical Atg9 vesicles, converting them into the disk-shaped isolation membranes.

To test whether Atg2 can transport lipids for Atg8 conjugation, we mixed two populations of liposomes. One population (SUV A) contained a lipid composition that efficiently recruited the lipidation machinery (*27*) but did not contain PE as substrate for Atg8 conjugation. The other population (SUV B) contained PE but was not efficiently targeted by the lipidation machinery (Fig. 4C and fig. S11C). Upon addition of Atg2-Atg18, which is active in lipid transport (fig. S11, A and B), we detected a significantly increased lipidation of Atg8, demonstrating that Atg2-Atg18 could directly enhance Atg8 lipidation (Fig. 4C). Because phosphatidylserine (PS) can also serve as substrate for Atg8 lipidation in vitro (*43*), the actual stimulatory effect of Atg2-Atg18 on Atg8 lipidation may be even higher. To exclude the possibility that Atg2-Atg18 allosterically activated the E3 by direct binding, we conjugated Atg8 to PE-containing SUVs in the presence or absence of Atg2-Atg18 and found that we could not observe significant differences in Atg8 lipidation (fig. S11D). Atg9 PLs also served as acceptors for Atg2-mediated lipid transport (Fig. 4D). We therefore sought to determine whether the lipids transported into Atg9 PLs could serve as substrates for Atg8 lipidation. Atg9 PLs lacking PE and PS were mixed with a second population of liposomes containing these lipids. We then added Atg2-Atg18 in the presence of the PI3KC3-C1, Atg21, Atg12–Atg5-Atg16, Atg7, Atg3, and Atg8 (Fig. 4E). We found that Atg8 lipidation, as monitored by immunoblotting, was accelerated in the presence of Atg2-Atg18 (Fig. 4E). To confirm that Atg8 lipidation occurred on the Atg9 PLs, we pulled down the Atg9 PLs using GFP-Trap beads and found lipidated Atg8 only in the presence of Atg2-Atg18 (Fig. 4E, arrow in top immunoblot).

Outlook

Here, we present a near-full in vitro reconstitution of the events occurring during autophagosome nucleation in selective autophagy. Specifically, we demonstrate that Atg9 vesicles are substrates of PI3KC3-C1 and that the PI3P generated in situ mediates the successive recruitment of Atg21, Atg2-Atg18, and the Atg12–Atg5-Atg16 complex as prerequisites for the subsequent Atg8 lipidation.

The role of Atg9 vesicles has remained mysterious. They are required for early steps of autophagosome formation but make up only a minor fraction of the lipids required to form the autophagosomal membrane (*8*–*11*). Autophagosomes are generated in proximity to the ER, but their membranes are clearly distinct from the ER membrane (*13*–*19*). Our results show that Atg9 vesicles form a platform for the recruitment of the autophagy machinery. Among them is the membrane tethering and lipid transfer protein Atg2 (*16*, *30*–*33*), which can transfer lipids at a rate that enables it to be a major contributor to isolation membrane expansion (*44*). It has become clear that lipid transfer at membrane contact sites provides the communication and membrane flow between intracellular compartments. However, lipid transfer can only occur between existing donor and acceptor compartments. Atg9 vesicles may thus form seeds for the initial establishment of membrane contact sites. Therefore, quantitative Atg8 lipidation may only occur after lipid influx from the ER into the Atg9 vesicle, gradually converting it into the disk-shaped isolation membrane (Fig. 5). In this manner, Atg9 vesicles could seed a biochemically distinctive membrane, the isolation membrane, largely devoid of transmembrane proteins (*45*, *46*). To ensure the expansion of the isolation membrane, the incoming lipids must be distributed to its inner leaflet, an action that would require flippase or scramblase activity. Notably, we found two flippases (Drs2 and Neo1) present in our Atg9 vesicle proteomics analysis. Multiple individual nucleation events followed by ESCRT (endosomal sorting complexes required for transport)–mediated membrane sealing may be required for the formation of larger autophagosomes (*47*–*49*).

In addition, the Golgi-derived Atg9 vesicles isolated from cells might be tightly packed with proteins. The influx of loosely packed lipids from the ER might thus render them good substrates for subsequent Atg8 lipidation apart from the expansion of the free membrane area. In fact, autophagosomal membranes contain a high proportion of lipids with unsaturated fatty acids (*12*). Apart from serving as acceptors

for lipid influx, Atg9 vesicles may also kickstart local lipid synthesis (*12*). Accordingly, we found Faa1 and Faa4 in our Atg9 vesicle proteomics.

During selective autophagy, cargo material is specifically sequestered by autophagosomes. It has become clear that cargo receptors act upstream of the autophagy machinery by recruiting scaffold proteins to the cargo (*50*–*56*). Here, we fully reconstitute the cargo receptor and scaffold dependent recruitment of the autophagy machinery to the cargo material and demonstrate that this system is sufficient to promote local Atg8 lipidation. Future work will reveal how the recruitment of the autophagy machinery, including the Atg9 vesicles, is sterically and temporally coupled to the formation of membrane contact sites with the ER.

Materials and methods summary

The full version of the materials and methods is available in the supplementary materials.

Protein expression and purification

Atg19 (residues 1 to 374) and the Atg19-3D and Atg19-3DΔLIR mutants were expressed and purified as described elsewhere (*57*, *58*). mEGFP/mCherry-Atg8-ΔR117 was expressed and purified as described in (*27*).

6xHis-TEV-Atg21, 6xHis-TEV-mEGFP-Atg21, 6xHis-TEV-mCherry-Atg21, 6xHis-Atg18-mEGFP, and Atg9-NTD(1-285)-mEGFP were all expressed in *E. coli* Rosetta pLysS.

Atg2-Atg18-CBP (CBP, calmodulin binding protein), Atg2-GFP-Atg18-CBP, and Atg2-mCherry-Atg18-CBP were purified from the SMY373, SMY374, and SMY439 yeast strains, respectively.

6xHis-TEV-Atg2-mEGFP, PI3KC3-C1, protA-TEV-Atg1-Atg13, 6xHis-TEV-mEGFP/mCherry-Atg11, and 6xHis-TEV-Atg9- mEGFP/mCherry were all expressed in the baculovirus expression system.

All soluble proteins were purified via affinity chromatography followed by size-exclusion chromatography.

For full length Atg9-mEGFP/mCherry, cell membranes were collected by centrifuging the cleared cell lysate at 40,000 revolutions per minute (rpm) for 1 hour. The membranes were resuspended for 2 hours at 4°C in lysis buffer containing 2% n-dodecyl β-D-maltoside (DDM). After 2 hours of incubation, the insoluble material was removed by centrifugation at 40,000 rpm for 1 hour. Atg9 was then purified by affinity chromatography followed by size-exclusion chromatography in the presence of 0.2% DDM. To concentrate the protein without increasing the detergent concentration, the fractions containing protein were incubated with 150 μl of nickel nitrilotriacetic acid (NiNTA) beads for 3 hours at 4°C. The beads were washed several times with 25 mM Tris pH 7.4, 300 mM NaCl, 0.04% DDM. The protein was eluted in the desired volume of buffer supplemented with 300 mM imidazole. A final dialysis was performed overnight at 4°C against 25 mM Tris pH 7.4, 300 mM NaCl, 0.04% DDM.

Atg9 PLs formation and analysis

Small unilamellar vesicles (SUVs; i.e., liposomes) destined for the reconstitution of Atg9 PLs were prepared with a lipid composition mimicking the lipid composition of the endogenous Atg9 vesicles determined in this study (for details, see table S2). For the incorporation of Atg9, the SUVs were treated with 3-[(3-cholamidopropyl)dimethylammonio]-1-propanesulfonate (CHAPS) (Avanti Polar Lipids, Inc.). The SUV suspension was brought up to 2.5% CHAPS and incubated at room temperature (RT) for 1 hour. The SUV suspension was then mixed at a 1:1 ratio with a 1-μM Atg9 solution in 0.04% DDM. The mixture was incubated at RT for another 90 min and then diluted by a factor of 10 in Tris 25 mM Tris pH 7.4, 300 mM NaCl to reach a detergent concentration below the critical micelle concentration (CMC) of both detergents. The resulting PL solution was dialyzed overnight at 4°C against 25 mM Tris pH 7.4, 300 mM NaCl supplemented with 0.1 g of BioBeads SM2 (BioRad) per liter of buffer. Finally, BioBeads were added directly to the sample and incubated for 1 hour at RT. The insoluble material that did not get incorporated into liposomes was removed by centrifuging 30 min at 18,000 rpm. The supernatant containing Atg9 PLs was collected and used for subsequent experiments.

Membrane recruitment—GUV assays

To image Atg21, Atg2-Atg18, and Atg12–Atg5-Atg16 membrane recruitment, 15 μl of the electroformed GUVs were transferred to a 96-well glass-bottom microplate (Greiner Bio-One), and the respective proteins were added to the final concentration of 1 μM in a final reaction volume of 30 μl in a reaction buffer 25 mM 4-(2-hydroxyethyl)-1-piperazineethanesulfonic acid (HEPES) at pH 7.5, 150 mM NaCl. In every experiment involving GUVs, before the GUVs and proteins were pipetted onto the plate, the wells were blocked with a blocking solution [2.5 mg/ml bovine serum albumin (BSA) in 50 mM TrisHCl pH 7.4, 150 mM NaCl] for 1 hour and washed twice with the reaction buffer.

For Atg21, Atg2-Atg18, and Atg12–Atg5-Atg16 membrane recruitment in the presence of PI3KC3-C1 experiments, mixes containing respective proteins, 0.1 mM adenosine triphosphate (ATP) or 0.1 mM adenylyl-imidodiphosphate (AMP-PNP), 0.5 mM $MgCl_2$, 2 mM $MnCl_2$, and 1 mM egtazic acid (EGTA) in a final volume of 15 μl were prepared. The final concentration of proteins in the reaction mixes were 50 nM for PI3KC3-C1, 400 nM for Atg21, 400 nM for Atg2-GFP-Atg18, and 40 nM for Atg12–Atg5-Atg16-mCherry. The reaction mixes were added to the well already containing 15 μl of the electroformed GUVs. For the time course experiment, the imaging started 5 min after the addition of the reaction mix to GUVs. The images were acquired for 45 min at the indicated time points of reaction.

In vitro reconstitution of Atg8 lipidation on GUVs

To image the PI3KC3-C1–dependent Atg8–PE conjugation to GUVs, mixes containing respective proteins (according to the experimental setup), 0.5 mM ATP, 0.5 mM $MgCl_2$, 2 mM $MnCl_2$, and 1 mM EGTA in a final volume of 15 μl were prepared. The reaction buffer contained 25 mM HEPES at pH 7.5, 150 mM NaCl. The final concentrations of proteins in the reaction mixes were 50 nM for PI3KC3-C1, 400 nM for Atg21, 400 nM for Atg2-Atg18, 40 nM for Atg12–Atg5-Atg16-mCherry, 80 nM for Atg7, 80 nM for Atg3, 400 nM GFP-Atg8ΔR117, and 400 nM GFP-Atg8-6xHis. The reaction mixes were added to wells of a 96-well glass-bottom microplate (Greiner Bio-One) already containing 15 μl of the electroformed GUVs. Concentrations of proteins and cofactors used were calculated for the final 30 μl volume of the experiment.

Microscopy-based protein-protein interaction assay

For the experiments shown in Fig. 2, B and G, giant unilamellar vesicles (GUVs) were prepared. Preparation was carried out as described above. Assays were performed under equilibrium conditions, and mEGFP-Atg21, 6xHis-Atg21, Atg12–Atg5-Atg16-mCherry, and Atg2-GFP-Atg18-CBP were added at a final concentration of 500 nM.

For Fig. 1, D to F, Atg12–Atg5-Atg16-mCherry, Atg5-mCherry-Atg16(1-46), and Atg16-mCherry were recruited to red fluorescent protein (RFP)–TRAP beads (Chromotek). Assays were performed under equilibrium conditions with 2 μM of the prey proteins Atg2-GFP-Atg18-CBP, Atg2-mEGFP, and Atg18-mEGFP.

Isolation of endogenous Atg9 vesicles

To isolate endogenous Atg9 vesicles, we cloned versions of Atg9 tagged with a fluorophore (mEGFP or mCherry) and a tobacco etch virus (TEV) cleavable affinity tag (9xmyc or TAP). These constructs were used to replace the endogenous *ATG9* gene in haploid BY474x *S. cerevisiae* cells, putting the expression under the control of the endogenous *ATG9* promoter. Constructs were then integrated into wild type or *pep4*Δ strains.

Strains were grown, harvested, and lysed. Cleared cell lysate was incubated with the appropriate affinity beads (coated with either immunoglobulin G or anti-myc antibody) at 4°C for 1 hour. The beads were then washed, the vesicles were released by TEV cleavage at 4°C for an hour, and the supernatant was collected.

In vitro reconstitution of Atg8 lipidation on Atg9 PLs or Atg9 vesicles bound to cargo-mimetic beads

Assembly of the cargo-mimetic beads

Glutathione sepharose 4B beads (GE Healthcare) were first equilibrated in 25 mM Tris pH 7.4, 300 mM NaCl. Beads were mixed with the same volume of a 30-μM solution of GST-prApe1 (1-41), 30-μM solution of Atg19-3DΔLIR mutant, and 30 μM of Atg11. The mixture was incubated for 1 hour at 4°C, and the beads were subsequently washed three times.

Recruitment of Atg9 PLs or Atg9 vesicles to the cargo-mimetic beads

Ten microliters of cargo-mimetic beads were mixed with either 200 μl of Atg9-mCherry PLs solution or an equal volume of TEV-eluted Atg9-EGFP vesicles. The mixture was incubated for 2 hours at 4°C, and the beads were subsequently washed once

In vitro Atg8 lipidation

Five tenths of a microliter of cargo-mimetic beads coated with Atg9-mCherry PL or Atg9-EGFP vesicles were pipetted into the wells of a 384-well glass-bottom microplate (Greiner Bio-One) containing 0.5 mM ATP, 0.5 mM $MgCl_2$, 2 mM $MnCl_2$, and 1 mM EGTA in a final volume of 15 μl. The final concentrations of proteins in the reaction mixes were 50 nM for PI3KC3-C1, 400 nM for Atg21, 400 nM for Atg2-Atg18, 40 nM for Atg12–Atg5-Atg16, 100 nM for Atg7, 100 nM for Atg3, and 400 nM for EGFP-Atg8ΔR117 (200 nM of mCherry-Atg8ΔR117 for Atg9 vesicles). The reactions were incubated for 2 hours at RT in the dark, and the beads were imaged using confocal microscope LSM700 (Zeiss) with 20× objective and processed with ImageJ software.

To deconjugate Atg8 from Atg9 vesicles, Atg4 or Atg4C147S was added at a final concentration of 0.5 μM together with EDTA at a final concentration of 2 mM, and microscopy images were taken at the indicated time points.

REFERENCES AND NOTES

1. N. Mizushima, M. Komatsu, Autophagy: Renovation of cells and tissues. *Cell* **147**, 728–741 (2011). doi: 10.1016/j.cell.2011.10.026; pmid: 22078875
2. B. Levine, G. Kroemer, Biological functions of autophagy genes: A disease perspective. *Cell* **176**, 11–42 (2019). doi: 10.1016/j.cell.2018.09.048; pmid: 30633901
3. Z. Xie, D. J. Klionsky, Autophagosome formation: Core machinery and adaptations. *Nat. Cell Biol.* **9**, 1102–1109 (2007). doi: 10.1038/ncb1007-1102; pmid: 17909521
4. N. Mizushima, T. Yoshimori, Y. Ohsumi, The role of Atg proteins in autophagosome formation. *Annu. Rev. Cell Dev. Biol.* **27**, 107–132 (2011). doi: 10.1146/annurev-cellbio-092910-154005; pmid: 21801009
5. C. A. Lamb, T. Yoshimori, S. A. Tooze, The autophagosome: Origins unknown, biogenesis complex. *Nat. Rev. Mol. Cell Biol.* **14**, 759–774 (2013). doi: 10.1038/nrm3696; pmid: 24201109
6. E. Turco, D. Fracchiolla, S. Martens, Recruitment and activation of the ULK1/Atg1 kinase complex in selective autophagy. *J. Mol. Biol.* **432**, 123–134 (2020). doi: 10.1016/j.jmb.2019.07.027; pmid: 31351898
7. G. Zaffagnini, S. Martens, Mechanisms of selective autophagy. *J. Mol. Biol.* **428**, 1714–1724 (2016). doi: 10.1016/j.jmb.2016.02.004; pmid: 26876603
8. H. Yamamoto *et al.*, Atg9 vesicles are an important membrane source during early steps of autophagosome formation. *J. Cell Biol.* **198**, 219–233 (2012). doi: 10.1083/jcb.201202061; pmid: 22826123
9. A. Orsi *et al.*, Dynamic and transient interactions of Atg9 with autophagosomes, but not membrane integration, are required for autophagy. *Mol. Biol. Cell* **23**, 1860–1873 (2012). doi: 10.1091/mbc.e11-09-0746; pmid: 22456507
10. A. R. J. Young *et al.*, Starvation and ULK1-dependent cycling of mammalian Atg9 between the TGN and endosomes. *J. Cell Sci.* **119**, 3888–3900 (2006). doi: 10.1242/jcs.03172; pmid: 16940348
11. Y. Ohashi, S. Munro, Membrane delivery to the yeast autophagosome from the Golgi-endosomal system. *Mol. Biol. Cell* **21**, 3998–4008 (2010). doi: 10.1091/mbc.e10-05-0457; pmid: 20861302
12. M. Schütter, P. Giavalisco, S. Brodesser, M. Graef, Local fatty acid channeling into phospholipid synthesis drives phagophore expansion during autophagy. *Cell* **180**, 135–149.e14 (2020). doi: 10.1016/j.cell.2019.12.005; pmid: 31883797
13. E. L. Axe *et al.*, Autophagosome formation from membrane compartments enriched in phosphatidylinositol 3-phosphate and dynamically connected to the endoplasmic reticulum. *J. Cell Biol.* **182**, 685–701 (2008). doi: 10.1083/jcb.200803137; pmid: 18725538
14. M. Graef, J. R. Friedman, C. Graham, M. Babu, J. Nunnari, ER exit sites are physical and functional core autophagosome biogenesis components. *Mol. Biol. Cell* **24**, 2918–2931 (2013). doi: 10.1091/mbc.e13-07-0381; pmid: 23904270
15. M. Hamasaki *et al.*, Autophagosomes form at ER-mitochondria contact sites. *Nature* **495**, 389–393 (2013). doi: 10.1038/nature11910; pmid: 23455425
16. R. Gómez-Sánchez *et al.*, Atg9 establishes Atg2-dependent contact sites between the endoplasmic reticulum and phagophores. *J. Cell Biol.* **217**, 2743–2763 (2018). doi: 10.1083/jcb.201710116; pmid: 29848619
17. M. Hayashi-Nishino *et al.*, A subdomain of the endoplasmic reticulum forms a cradle for autophagosome formation. *Nat. Cell Biol.* **11**, 1433–1437 (2009). doi: 10.1038/ncb1991; pmid: 19898463
18. P. Ylä-Anttila, H. Vihinen, E. Jokitalo, E.-L. Eskelinen, 3D tomography reveals connections between the phagophore and endoplasmic reticulum. *Autophagy* **5**, 1180–1185 (2009). doi: 10.4161/auto.5.8.10274; pmid: 19855179
19. T. Nishimura *et al.*, Autophagosome formation is initiated at phosphatidylinositol synthase-enriched ER subdomains. *EMBO J.* **36**, 1719–1735 (2017). doi: 10.15252/embj.201695189; pmid: 28495679
20. H. Wu, P. Carvalho, G. K. Voeltz, Here, there, and everywhere: The importance of ER membrane contact sites. *Science* **361**, eaan5835 (2018). doi: 10.1126/science.aan5835; pmid: 30072511
21. S. Cohen, A. M. Valm, J. Lippincott-Schwartz, Interacting organelles. *Curr. Opin. Cell Biol.* **53**, 84–91 (2018). doi: 10.1016/j.ceb.2018.06.003; pmid: 30006038
22. Y. Ichimura *et al.*, A ubiquitin-like system mediates protein lipidation. *Nature* **408**, 488–492 (2000). doi: 10.1038/35044114; pmid: 11100732
23. Y. Kabeya *et al.*, LC3, a mammalian homologue of yeast Apg8p, is localized in autophagosome membranes after processing. *EMBO J.* **19**, 5720–5728 (2000). doi: 10.1093/emboj/19.21.5720; pmid: 11060023
24. M. R. Slobodkin, Z. Elazar, The Atg8 family: Multifunctional ubiquitin-like key regulators of autophagy. *Essays Biochem.* **55**, 51–64 (2013). doi: 10.1042/bse0550051; pmid: 24070471
25. T. Hanada *et al.*, The Atg12-Atg5 conjugate has a novel E3-like activity for protein lipidation in autophagy. *J. Biol. Chem.* **282**, 37298–37302 (2007). doi: 10.1074/jbc.C700195200; pmid: 17986448
26. Y. Zheng *et al.*, A switch element in the autophagy E2 Atg3 mediates allosteric regulation across the lipidation cascade. *Nat. Commun.* **10**, 3600 (2019). doi: 10.1038/s41467-019-11435-y; pmid: 31399562
27. J. Romanov *et al.*, Mechanism and functions of membrane binding by the Atg5-Atg12/Atg16 complex during autophagosome formation. *EMBO J.* **31**, 4304–4317 (2012). doi: 10.1038/emboj.2012.278; pmid: 23064152
28. N. Fujita *et al.*, The Atg16L complex specifies the site of LC3 lipidation for membrane biogenesis in autophagy. *Mol. Biol. Cell* **19**, 2092–2100 (2008). doi: 10.1091/mbc.e07-12-1257; pmid: 18321988
29. L. Juris *et al.*, PI3P binding by Atg21 organises Atg8 lipidation. *EMBO J.* **34**, 955–973 (2015). doi: 10.15252/embj.201488957; pmid: 25691244
30. K. Obara, T. Sekito, K. Niimi, Y. Ohsumi, The Atg18-Atg2 complex is recruited to autophagic membranes via phosphatidylinositol 3-phosphate and exerts an essential function. *J. Biol. Chem.* **283**, 23972–23980 (2008). doi: 10.1074/jbc.M803180200; pmid: 18586673
31. D. P. Valverde *et al.*, ATG2 transports lipids to promote autophagosome biogenesis. *J. Cell Biol.* **218**, 1787–1798 (2019). doi: 10.1083/jcb.201811139; pmid: 30952800
32. T. Osawa *et al.*, Atg2 mediates direct lipid transfer between membranes for autophagosome formation. *Nat. Struct. Mol. Biol.* **26**, 281–288 (2019). doi: 10.1038/s41594-019-0203-4; pmid: 30911189
33. T. Kotani, H. Kirisako, M. Koizumi, Y. Ohsumi, H. Nakatogawa, The Atg2-Atg18 complex tethers pre-autophagosomal membranes to the endoplasmic reticulum for autophagosome formation. *Proc. Natl. Acad. Sci. U.S.A.* **115**, 10363–10368 (2018). doi: 10.1073/pnas.1806727115; pmid: 30254161
34. K. Harada *et al.*, Two distinct mechanisms target the autophagy-related E3 complex to the pre-autophagosomal structure. *eLife* **8**, e43088 (2019). doi: 10.7554/eLife.43088; pmid: 30810528
35. A. Kihara, T. Noda, N. Ishihara, Y. Ohsumi, Two distinct Vps34 phosphatidylinositol 3-kinase complexes function in autophagy and carboxypeptidase Y sorting in *Saccharomyces cerevisiae*. *J. Cell Biol.* **152**, 519–530 (2001). doi: 10.1083/jcb.152.3.519; pmid: 11157979
36. S. W. Suzuki *et al.*, Atg13 HORMA domain recruits Atg9 vesicles during autophagosome formation. *Proc. Natl. Acad. Sci. U.S.A.* **112**, 3350–3355 (2015). doi: 10.1073/pnas.1421092112; pmid: 25737544
37. G. van Meer, D. R. Voelker, G. W. Feigenson, Membrane lipids: Where they are and how they behave. *Nat. Rev. Mol. Cell Biol.* **9**, 112–124 (2008). doi: 10.1038/nrm2330; pmid: 18216768
38. C. He *et al.*, Recruitment of Atg9 to the preautophagosomal structure by Atg11 is essential for selective autophagy in budding yeast. *J. Cell Biol.* **175**, 925–935 (2006). doi: 10.1083/jcb.200606084; pmid: 17178909
39. N. Matscheko, P. Mayrhofer, Y. Rao, V. Beier, T. Wollert, Atg11 tethers Atg9 vesicles to initiate selective autophagy. *PLOS Biol.* **17**, e3000377 (2019). doi: 10.1371/journal.pbio.3000377; pmid: 31356628
40. H. Suzuki, N. N. Noda, Biophysical characterization of Atg11, a scaffold protein essential for selective autophagy in yeast. *FEBS Open Bio* **8**, 110–116 (2017). doi: 10.1002/2211-5463.12355; pmid: 29321961
41. T. Pfaffenwimmer *et al.*, Hrr25 kinase promotes selective autophagy by phosphorylating the cargo receptor Atg19. *EMBO Rep.* **15**, 862–870 (2014). doi: 10.15252/embr.201438932; pmid: 24968893
42. Z. Tang *et al.*, TOM40 targets Atg2 to mitochondria-associated ER membranes for phagophore expansion. *Cell Rep.* **28**, 1744–1757.e5 (2019). doi: 10.1016/j.celrep.2019.07.036; pmid: 31412244
43. K. Oh-oka, H. Nakatogawa, Y. Ohsumi, Physiological pH and acidic phospholipids contribute to substrate specificity in lipidation of Atg8. *J. Biol. Chem.* **283**, 21847–21852 (2008). doi: 10.1074/jbc.M801836200; pmid: 18544538
44. S. von Bülow, G. Hummer, Kinetics ofAtg2-mediated lipid transfer from the ER can account for phagophore expansion. bioRxiv 2020.05.12.090977 [Preprint]. 14 May 2020. https://doi.org/10.1101/2020.05.12.090977.
45. M. Baba, K. Takeshige, N. Baba, Y. Ohsumi, Ultrastructural analysis of the autophagic process in yeast: Detection of autophagosomes and their characterization. *J. Cell Biol.* **124**, 903–913 (1994). doi: 10.1083/jcb.124.6.903; pmid: 8132712
46. M. Fengsrud, E. S. Erichsen, T. O. Berg, C. Raiborg, P. O. Seglen, Ultrastructural characterization of the delimiting membranes of isolated autophagosomes and amphisomes by freeze-fracture electron microscopy. *Eur. J. Cell Biol.* **79**, 871–882 (2000). doi: 10.1078/0171-9335-00125; pmid: 11152279
47. Y. Takahashi *et al.*, An autophagy assay reveals the ESCRT-III component CHMP2A as a regulator of phagophore closure. *Nat. Commun.* **9**, 2855 (2018). doi: 10.1038/s41467-018-05254-w; pmid: 30030437
48. Y. Zhen *et al.*, ESCRT-mediated phagophore sealing during mitophagy. *Autophagy* **16**, 826–841 (2020). doi: 10.1080/15548627.2019.1639301; pmid: 31366282
49. F. Zhou *et al.*, Rab5-dependent autophagosome closure by ESCRT. *J. Cell Biol.* **218**, 1908–1927 (2019). doi: 10.1083/jcb.201811173; pmid: 31010855
50. B. J. Ravenhill *et al.*, The cargo receptor NDP52 initiates selective autophagy by recruiting the ULK complex to cytosol-invading bacteria. *Mol. Cell* **74**, 320–329.e6 (2019). doi: 10.1016/j.molcel.2019.01.041; pmid: 30853402

51. M. D. Smith, S. Wilkinson, CCPG1, an unconventional cargo receptor for ER-phagy, maintains pancreatic acinar cell health. *Mol. Cell. Oncol.* **5**, e1441631 (2018). doi: 10.1080/23723556.2018.1441631; pmid: 30263939
52. J. N. S. Vargas *et al*., Spatiotemporal control of ULK1 activation by NDP52 and TBK1 during selective autophagy. *Mol. Cell* **74**, 347–362.e6 (2019). doi: 10.1016/j.molcel.2019.02.010; pmid: 30853401
53. E. Turco *et al*., FIP200 claw domain binding to p62 promotes autophagosome formation at ubiquitin condensates. *Mol. Cell* **74**, 330–346.e11 (2019). doi: 10.1016/j.molcel.2019.01.035; pmid: 30853400
54. T. Shintani, D. J. Klionsky, Cargo proteins facilitate the formation of transport vesicles in the cytoplasm to vacuole targeting pathway. *J. Biol. Chem.* **279**, 29889–29894 (2004). doi: 10.1074/jbc.M404399200; pmid: 15138258
55. R. A. Kamber, C. J. Shoemaker, V. Denic, Receptor-bound targets of selective autophagy use a scaffold protein to activate the Atg1 kinase. *Mol. Cell* **59**, 372–381 (2015). doi: 10.1016/j.molcel.2015.06.009; pmid: 26166702
56. R. Torggler *et al*., Two independent pathways within selective autophagy converge to activate Atg1 kinase at the vacuole. *Mol. Cell* **64**, 221–235 (2016). doi: 10.1016/j.molcel.2016.09.008; pmid: 27768871
57. D. Fracchiolla *et al*., Mechanism of cargo-directed Atg8 conjugation during selective autophagy. *eLife* **5**, e18544 (2016). doi: 10.7554/eLife.18544; pmid: 27879200
58. J. Sawa-Makarska *et al*., Cargo binding to Atg19 unmasks additional Atg8 binding sites to mediate membrane-cargo apposition during selective autophagy. *Nat. Cell Biol.* **16**, 425–433 (2014). doi: 10.1038/ncb2935; pmid: 24705553

ACKNOWLEDGMENTS

We thank G. Warren for comments on the manuscript. We thank S. Brodesser and the CECAD Lipidomics/Metabolomics Facility for performing lipidomics analyses. We thank M. Hartl from the Max Perutz Labs Mass Spectrometry Facility, the Max Perutz Labs BioOptics Facility, and the VBCF Electron Microscopy Facility for technical support and the VBCF for providing the MS instrument pool. Anti-CBP antibody and yeast strains carrying Atg2-Atg18 expression cassettes were provided by C. Ungermann. We thank L. Pietrek for help with the simulation setup and D. Fracchiolla for expressing and purifying unlabeled Atg21. **Funding:** This work was supported by ERC grant 646653 (S.M.), Austrian Science Fund FWF P32814-B (S.M.) and T724-B20 (J.S.-M.), Human Frontier Science Program RGP0026/2017 (S.M., G.H., and S.v.B.), an OEAW Doc fellowship (C.A.), and the Max Planck Society (G.H., S.v.B., and M.G.). **Author contributions:** S.M., J.S.-M., and G.H. designed and supervised research. V.B., N.C., S.v.B., and V.N. designed research. J.S.-M., V.B., N.C., S.v.B., V.N., C.A., and M.S. performed research. All authors analyzed data and commented on the manuscript. S.M. and J.S.-M. wrote the manuscript. **Competing interests:** S.M. is a member of the scientific advisory board of Casma Therapeutics. **Data and materials availability:** All data are available in the manuscript or the supplementary materials.

SUPPLEMENTARY MATERIALS

science.sciencemag.org/content/369/6508/eaaz7714/suppl/DC1
Materials and Methods
Figs. S1 to S11
Tables S1 to S5
References (*59*–*95*)
MDAR Reproducibility Checklist
Movie S1
Data S1

View/request a protocol for this paper from *Bio-protocol*.

9 October 2019; resubmitted 16 May 2020
Accepted 6 July 2020
10.1126/science.aaz7714

Reconstitution of autophagosome nucleation defines Atg9 vesicles as seeds for membrane formation

Justyna Sawa-Makarska, Verena Baumann, Nicolas Coudevylle, Sören von Bülow, Veronika Nogellova, Christine Abert, Martina Schuschnig, Martin Graef, Gerhard Hummer and Sascha Martens

Science **369** (6508), eaaz7714.
DOI: 10.1126/science.aaz7714

Reconstituting autophagosome nucleation

To stay healthy, our cells must constantly dispose of harmful material. Autophagy, or self-eating, is an important mechanism to ensure the clearance of bulky material. Such material is enwrapped by cellular membranes to form autophagosomes, the contents of which are then degraded. The formation of autophagosomes is a complicated process involving a large number of factors. How they act together in this process is still enigmatic. Sawa-Makarska *et al.* recapitulated the initial steps of autophagosome formation using purified autophagy factors from yeast. This approach elucidated some of the organizational principles of the autophagy machinery during the assembly of autophagosomes.

Science, this issue p. eaaz7714